RSC Sustainability

ROYAL SOCIETY OF CHEMISTRY

PAPER

View Article Online
View Journal | View Issue

Cite this: *RSC Sustainability*, 2024, **2**, 2615

A cooperative nanoscale ZnO–NiO–Ni heterojunction for sustainable catalytic amidation of aldehydes with secondary amines†

Amishwar Raysing Shelte,[ab] Rahul Daga Patil[ab] and Sanjay Pratihar *[ab]

Metal–metal hydroxide/oxide interface catalysts are valued for their multiple active sites, enabling synergistic reactions in close proximity for advanced catalytic applications. Herein, we present a highly efficient and sustainable method for synthesizing amides through oxidative amidation reactions involving aldehydes and secondary amines. The method utilizes *tert*-butyl hydroperoxide (TBHP) as the oxidant in THF at 90 °C and employs well-defined nanoscale heterojunctions of zinc oxide, nickel oxide, nickel [ZnO–NiO–Ni] (**ZN-O-A-7**) as a recyclable heterogeneous catalyst. The ZnO–NiO–Ni heterostructure and their synergistic cooperation are crucial for enhancing the efficiency and selectivity of the oxidative amidation reaction. The versatility of the methodology was demonstrated with diverse aldehyde derivatives and secondary amines, including morpholine, thiomorpholine, piperazine, pyrrolidine, and piperidine. Mechanistic investigations *via* controlled experiments provided insights into the underlying processes. The catalyst demonstrates ease of synthesis, use of stoichiometric amounts of oxidant, excellent selectivity, high functional group tolerance, applicability to various aldehydes and amines, multiple reusability, and potential for large-scale processes. These features collectively enhance the economic and sustainable nature of both the catalyst and the protocol, making a valuable contribution to the field of catalytic amidation reactions.

Received 13th June 2024
Accepted 17th July 2024

DOI: 10.1039/d4su00304g

rsc.li/rscsus

Sustainability spotlight

Amides are vital in pharmaceuticals, agrochemicals, and materials science but face synthetic challenges. We developed a recyclable ZnO–NiO–Ni catalyst for oxidative amidation, displaying high functional group tolerance, multiple reusability, and good activity across a broad substrate scope. It effectively utilizes diverse aldehyde derivatives and secondary amines, including morpholine, thiomorpholine, piperazine, pyrrolidine, and piperidine. Evaluated using CHEM21 metrics, our method excels in yield, atom economy, and mass efficiency, using less oxidant than reported methodologies. It aligns with UN SDGs industry, innovation, and infrastructure (SDG 9), responsible consumption and production (SDG 12), and climate action (SDG 13). Our work advances sustainable chemistry and underscores our commitment to environmental stewardship.

Introduction

Amides are crucial structural motifs in various natural products, peptides, proteins, agrochemicals, and pharmaceuticals. They are also extensively used in detergents, pigments, lubricants, and synthetic polymers.[1–6] Typically, the synthesis of amides involves acylating amines with carboxylic acid derivatives or condensing carboxylic acids with amines. These processes often require coupling agents or the conversion of reactants into more reactive derivatives.[7–11] Nevertheless, these approaches come with inherent limitations, including the production of a stoichiometric quantity of by-products and the use of potentially hazardous reagents.[12] An alternative method for synthesizing amides is oxidative amidation, which involves the direct amidation of aldehydes with amines.[13,14] This approach has demand due to its considerations for atom economy and green chemistry principles.[15–17] In this process, equivalent amounts of aldehyde and amine are coupled to form the corresponding amide. Nakagawa and co-workers initially reported the oxidative amidation of aldehydes with amines, using a stoichiometric amount of nickel peroxide.[18] Furthermore, catalysts have been reported based on transition metals such as ruthenium,[19] rhodium,[20] palladium,[20] copper,[21,22] nickel,[23] and gold.[24] While these pioneering reports have introduced efficient and environmentally favorable methods for amide formation, certain reactions require the use of expensive and hazardous dual catalysts. Moreover, the separation of

[a]*Inorganic Materials and Catalysis Division, CSIR-Central Salt & Marine Chemicals Research Institute, Gijubhai Badheka Marg, Bhavnagar, Gujarat 364002, India. E-mail: spratihar@csmcri.res.in; spratihar29@gmail.com*

[b]*Academy of Scientific and Innovative Research (AcSIR), Ghaziabad, 201002, India*

† Electronic supplementary information (ESI) available: Detailed experimental procedures, controlled studies, synthesis, characterization, ^{1}H and ^{13}C NMR spectra, and XPS spectra (PDF). See DOI: https://doi.org/10.1039/d4su00304g

homogeneous catalysts like $Cu(OAc)_2$ (ref. 25) and $CuCl_2$ (ref. 26) poses challenges, and these catalysts are often non-recyclable in many cases. Therefore, pursuing a more cost-effective, environmentally friendly, heterogeneous, and simpler catalyst system remains a significant challenge. Rostamnia and co-workers reported Pd nanoparticles supported on graphene oxide for oxidative amidation of an aldehyde and 2-aminopyridine.[27] A copper-MOF for the oxidative amidation of aldehydes and amines in a single pot for the synthesis of amides was reported by Mokhtari and colleagues.[28] Rajabi and co-workers reported the use of supported cobalt oxide nanoparticles as an efficient catalyst for amidation and esterification reactions.[29] Besides Pd, Cu, and Co, heterogeneous nickel-based catalysts were utilized for oxidative amidation of benzaldehyde with an amine to synthesize an important amide scaffold. A NiO@Ni Mott–Schottky catalyst developed from a metal–organic framework was presented by Jain and colleagues for the oxidative amidation of aldehydes with amines under mild reaction conditions.[30] Kargar and colleagues reported on the effective and recyclable use of a porous metal–organic framework (Ni-MOF) as a catalyst for the cascade oxidative amidation of alcohols by amines under ultrasonic irradiation.[31] Recently, Zhao and colleagues reported the direct synthesis of amides from the oxidative coupling of aldehydes with *N*-substituted formamides using a Co–Ni-CM heterogeneous catalyst.[32] A Ni-based metal–organic framework was reported by Nguyen *et al.* to be an effective catalyst for the amidation process.[33] Recent studies have shown an increased use of metal and metal oxide nanoparticles to investigate a wide range of organic transformations.[34] Enhancing the surface area, constructing specific crystal phases, and altering the size and shape of nanoparticles can significantly improve their effectiveness.

We present a highly efficient and sustainable method for synthesizing amides *via* oxidative amidation of aldehydes and secondary amines. Utilizing *tert*-butyl hydroperoxide (TBHP) as the oxidant in THF at 90 °C, the reaction employs well-defined nanoscale heterojunctions of ZnO–NiO–Ni (**ZN-O-A-7**) as a recyclable heterogeneous catalyst.[35,36] This ZnO–NiO–Ni heterojunction significantly enhances the reaction efficiency and selectivity. The versatility of the method was demonstrated with various aldehydes and secondary amines, such as morpholine, thiomorpholine, piperazine, pyrrolidine, and piperidine. Mechanistic studies *via* controlled experiments revealed insights into the process, highlighting the catalyst's high functional group tolerance, broad substrate scope, reusability, and robust activity. Sustainability was evaluated using the CHEM21 green metrics toolkit, which shows that our method excels in yield, atom economy (AE), and reaction mass efficiency (RME), using less oxidant than reported methodologies.

Results and discussion

Characterization of materials

The materials used in this study have already been characterized and reported by us; however, to detail their characteristics and composition, we will briefly discuss their synthesis and characterization based on our previous reports.[35,36] **ZN-O**, displaying free/coordinated carboxylate and amide functionality, was formed by the reaction of a zinc–sodium acetate complex ($C_{32}H_{48}O_{34}Na_8Zn_4$, **C-1**) with hydrazine hydrate, as shown by high-resolution C 1s and N 1s spectra. Acetate decomposition between 310 and 360 °C and amide decomposition between 170 and 250 °C resulted in a weight loss of around 27.5% and 28.1%, respectively, according to thermogravimetric analysis (Fig. 2). Ni(II) reduction to Ni(0) and other redox processes are expected to be enhanced by the thermal decomposition carried out by pyrolysis, which will also affect the distribution, shape, and composition of the material. Zinc(II) may be reduced to Zn(0) by the thermal decomposition of organic moieties, but this is less likely to occur when nickel exists as zinc possesses a higher reducing capacity than nickel. ZnO appears to be present in **ZN-O** and **ZN-R** based on the XPS spectra, which show two distinct peaks with a binding energy difference (D_m) of around 23 eV for Zn 2p3/2 and Zn 2p1/2 within the range of 1016–1044 eV. Two large peaks with centers at 856 eV and 862 eV (with a satellite peak) are visible in the Ni 2p XPS spectra of **ZN-O** and **ZN-R**, respectively.[35] The peak at 856 eV was split into two sub-peaks: the signal of Ni(0) was found at a lower binding energy of 852.5 eV, while that of Ni(II) was found at 855.5 eV. **ZN-O** has an estimated nickel content of 11% and a zinc content of 24%, according to the ICP-MS analysis (Table 1). In **ZN-O**, the XPS analysis revealed an approximate nickel to zinc atomic ratio of 1 : 1.4. For **ZN-O** and **ZN-R**, the mean crystallite sizes were found to be 23 nm and 28 nm, respectively, using the Scherrer equation. According to PXRD, the *d*-spacings of the (111) crystal planes of NiO and the (100) and (002) planes of ZnO correlate with the reported fringe spacing for **ZN-O** in HR-TEM. Additionally, the **ZN-R** fringe

Table 1 Materials developed under various conditions and compositions from ZN-O and ZN-R

#	Materials[a]	Calcination conditions[b]	wt% Ni/Zn[c]	Ni(II)/Ni(0)[d]
1	**ZN-O**	60 °C, 12 h	14/35	91/9
2	**ZN-O-5**	500 °C, air	26/48	60/40
3	**ZN-O-7**	700 °C, air	21/47	55/45
4	**ZN-O-A-7**	700 °C, argon	21/48	51/49
5	**ZN-R**	60 °C, 12 h	14/35	94/06
6	**ZN-R-5**	500 °C, air	17/38	64/36
7	**ZN-R-A-7**	700 °C, argon	19/50	51/49

[a] The material produced when **C-1** and hydrazine hydrate reacts for 12 hours at 90 °C and 130 °C in a sealed Teflon tube is labeled as **ZN-O** and **ZN-R** is the material that is obtained when **ZN-O** and sodium borohydride react in water–methanol (10/10 mL) at room temperature (298 K) for 6 hours. The material is then recovered by centrifugation, cleaned with methanol and water, and vacuum-dried. **ZN-O-5** and **ZN-O-7** are the materials obtained after **ZN-O** is annealed in air at a temperature range of 500 to 700 °C respectively. [b] **ZN-O** and **ZN-R** were calcined under specific conditions, including air and argon for three hours at 500 and 700 °C. [c] The ICP-MS analysis of the reaction solution following acid digestion was used to determine the wt% of metals (Zn/Ni) in the materials. Each sample underwent three repetitions of the ICP-MS analysis, with standard deviations of ±0.5% for Zn and ±0.3% for Ni being observed. [d] The high-resolution XPS Ni 2p core level spectra analysis was used to determine the contents of Ni(II) and Ni(0) in various materials.

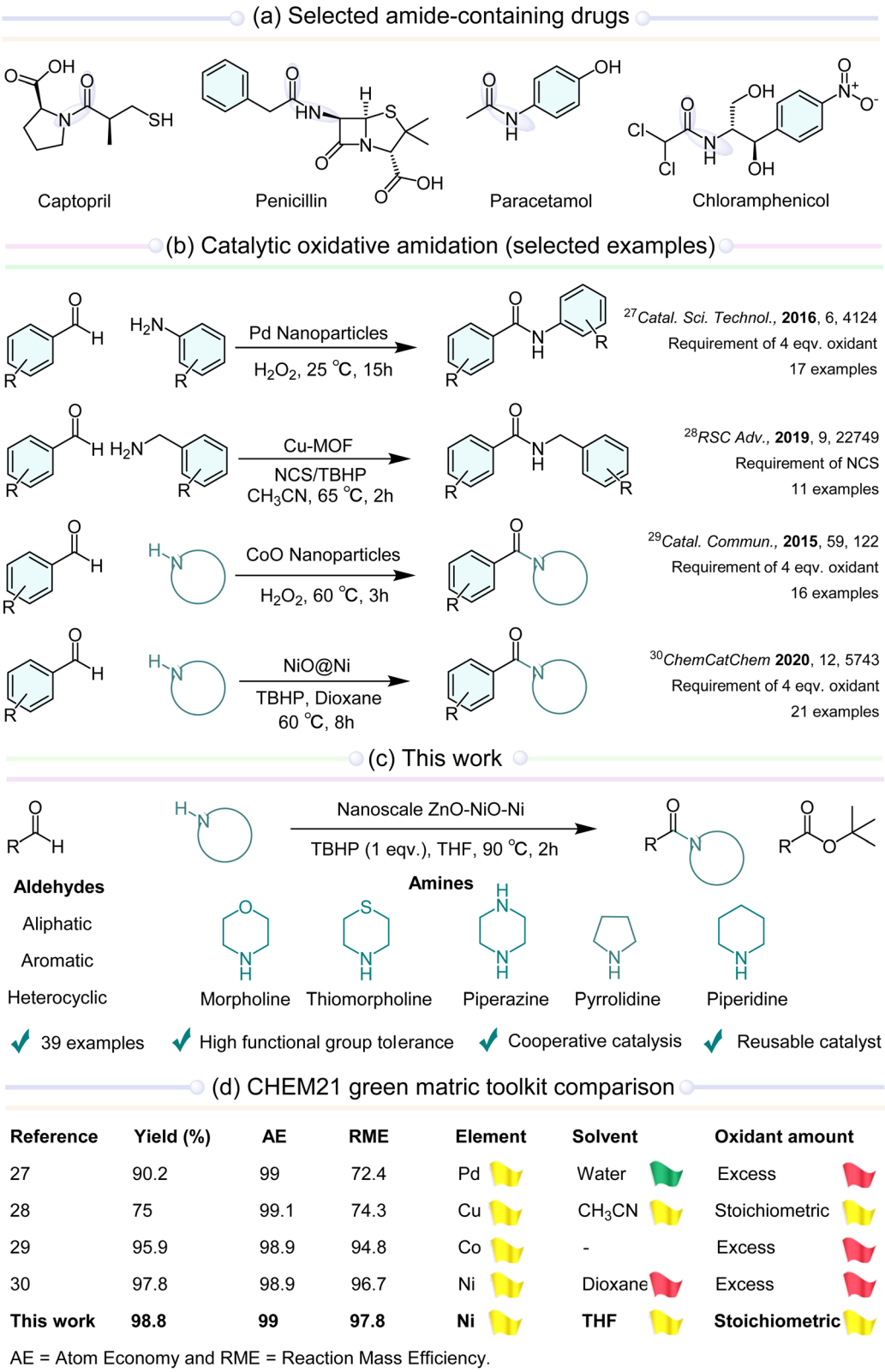

Reference	Yield (%)	AE	RME	Element	Solvent	Oxidant amount
27	90.2	99	72.4	Pd	Water	Excess
28	75	99.1	74.3	Cu	CH_3CN	Stoichiometric
29	95.9	98.9	94.8	Co	-	Excess
30	97.8	98.9	96.7	Ni	Dioxane	Excess
This work	**98.8**	**99**	**97.8**	**Ni**	**THF**	**Stoichiometric**

AE = Atom Economy and RME = Reaction Mass Efficiency.

Fig. 1 (a) Selected examples of amide-containing drugs; (b) catalytic oxidative amidation (selected examples); (c) this work; (d) CHEM21 green metrics toolkit comparison.

spacing corresponds to the (200) NiO and Ni crystal planes and the (100) ZnO planes. On the (111) and (200) crystal planes, NiO appears to form during the pyrolysis of **ZN-O** at 500 °C. ZnO, on the other hand, showed development on crystal planes (002) and (100). The irregular hexagonal rod-like structure was transformed into mostly hexagonal rods after pyrolysis, with

a mean crystallite size of 25 nm in **ZN-O-5** (Fig. 1). Lattice fringe spacings which are compatible with the *d*-spacings reported for the (111) and (200) crystal planes of NiO and (100) and (002) planes of ZnO were detected in the HR-TEM image of **ZN-O-5** obtained from the edge of the nanoparticle. According to this observation, ZnO and NiO may form a heterojunction. Ni(0)/Ni(II) was found to be roughly 40/60, and the nickel : zinc ratio of **ZN-O-5**, according to XPS analysis, was predicted to be around 1 : 1.5. **ZN-O** was annealed at 700 °C for three hours with a constant argon flow to increase the material's Ni(0) concentration (Table 1). Notably, the argon atmosphere promoted growth along the NiO (111) and ZnO (200) crystal planes and the ZnO (100) and (002) crystal planes. This resulted in the formation of a regular hexagon (**ZN-O-A-7**) that measured roughly 200–220 nm in length and 250–280 nm in diameter. The lattice fringe spacings in the HR-TEM image, which was taken from the edge of a hexagon (**ZN-O-A-7**), were in agreement with the previously published *d*-spacings for the NiO crystal planes (111 and 200), the Ni(0) planes (111 and 200), and the ZnO planes (100, 101, and 002). This observation points to the possibility of ZnO, NiO, and Ni(0) forming a heterojunction. Furthermore, ZnO, NiO, and Ni(0) were confirmed by XPS analysis to be present in **ZN-O-A-7**. Even after being exposed to higher temperatures, the Zn and Ni contents in **ZN-O-A-7**, which were roughly 45% and 25% by weight, respectively, remained relatively consistent. This shows that all of the material's volatile organic moieties have completely broken down. On the other hand, when **ZN-O** was reduced using sodium borohydride ($NaBH_4$), most of the organic matter was eliminated, including the coordinated amide and acetate functional groups. Thus, **ZN-R** was formed, which has a unique structure consisting of zinc and nickel hydroxides and oxides with trace amounts of Ni(0). 24 nm is the determined crystallite size of **ZN-R-5**. The flakes' initial aggregation was then altered by an argon environment at 700 °C, giving rise to **ZN-R-A-7**, which has a mean crystallite size of 20 nm and a hexagonal rod-like shape. The calculated ratio of Ni(0) to Ni(II) in **ZN-R-A-7** remained almost equal.

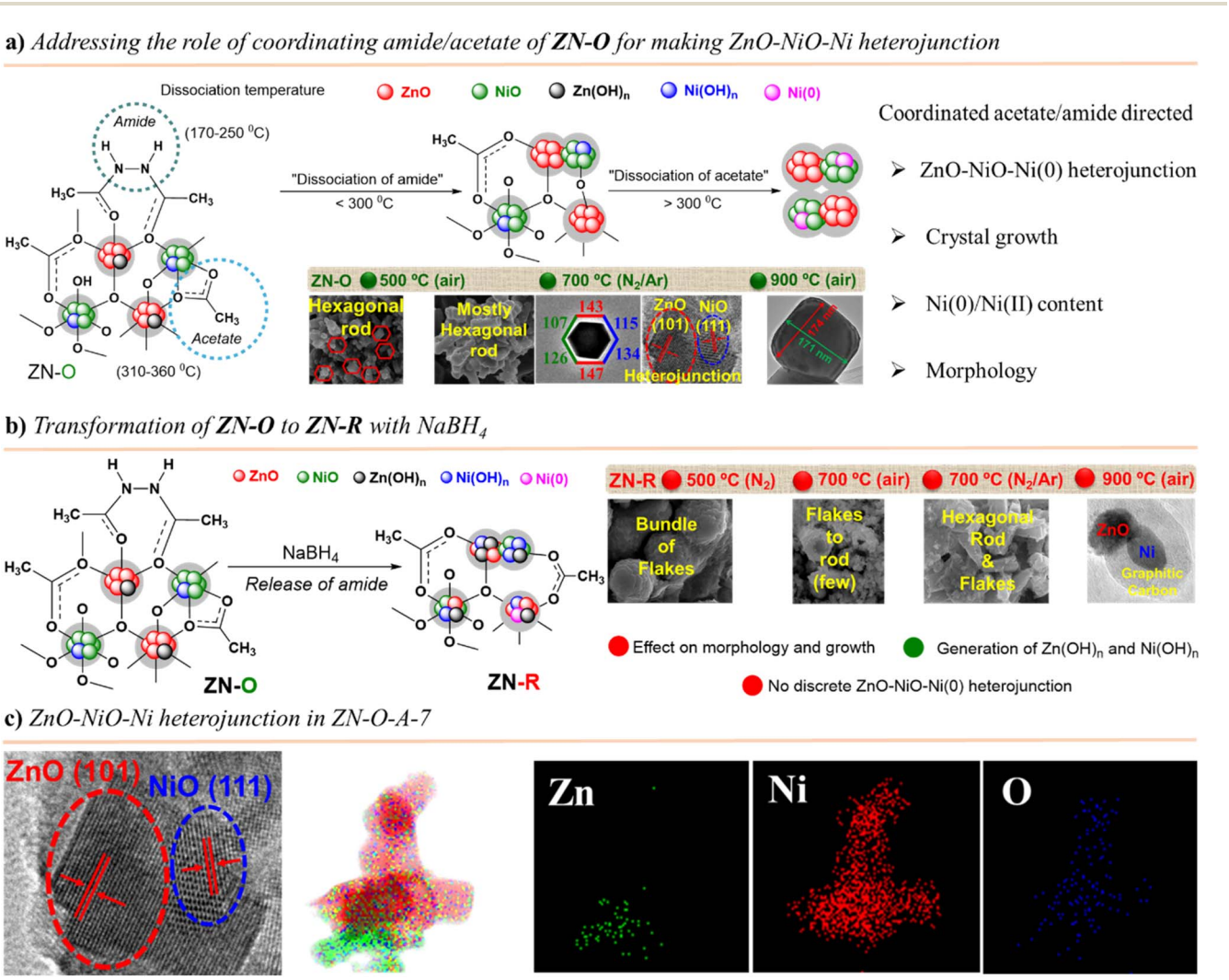

Fig. 2 Schematic diagram of the role of coordinating acetate/amide of **ZN-O** for ZnO–NiO–Ni(0) heterojunctions (a); schematic diagram representing the conversion of **ZN-O** to **ZN-R** along with HR-SEM and HR-TEM images of materials obtained from **ZN-R** at different temperatures and in different atmospheres (b); HR-TEM images and HR-TEM elemental mapping for the ZnO–NiO–Ni heterojunction (c).

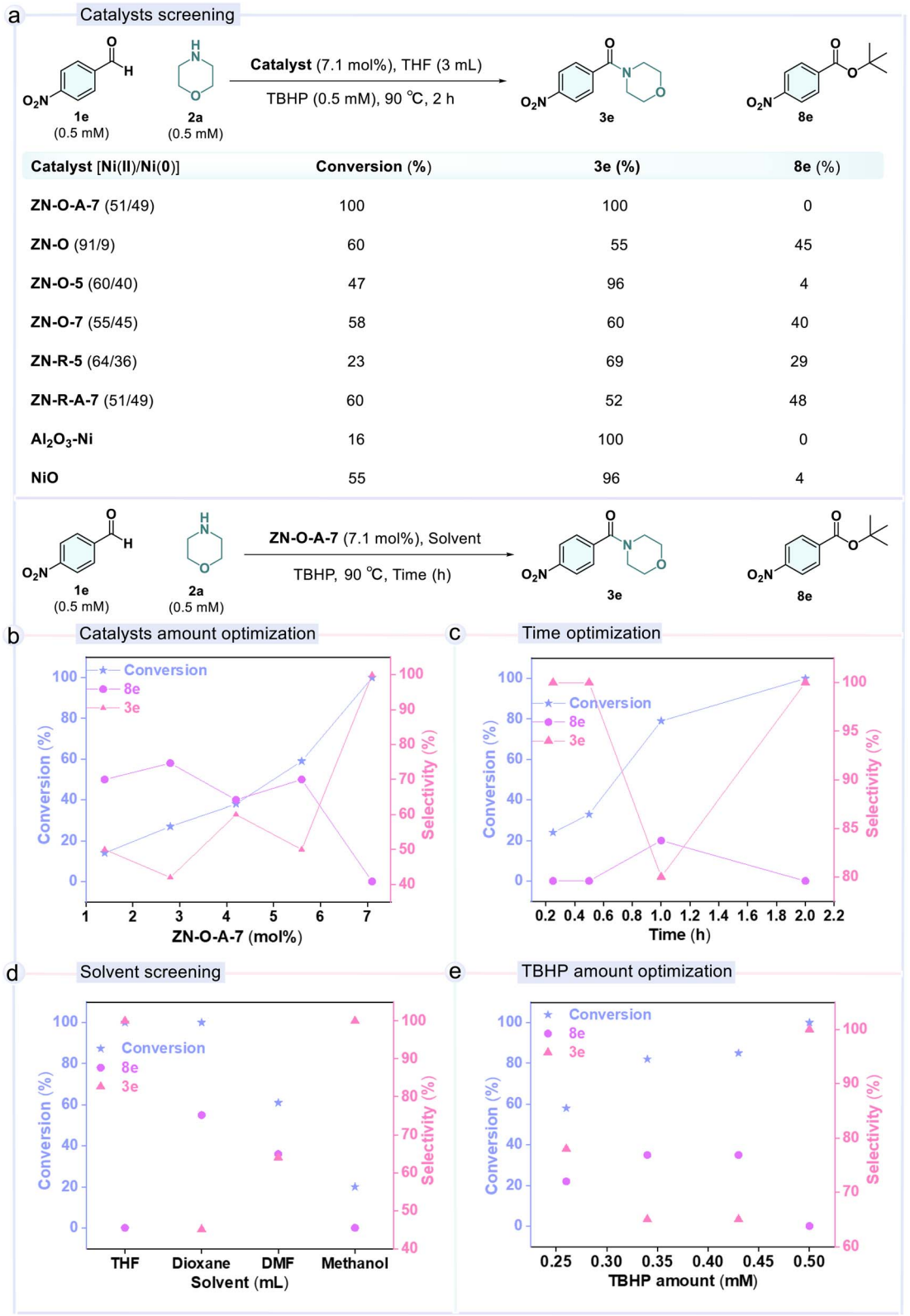

Catalyst [Ni(II)/Ni(0)]	Conversion (%)	3e (%)	8e (%)
ZN-O-A-7 (51/49)	100	100	0
ZN-O (91/9)	60	55	45
ZN-O-5 (60/40)	47	96	4
ZN-O-7 (55/45)	58	60	40
ZN-R-5 (64/36)	23	69	29
ZN-R-A-7 (51/49)	60	52	48
Al_2O_3-Ni	16	100	0
NiO	55	96	4

Fig. 3 Optimization of reaction conditions: (a) catalyst screening; (b) catalyst amount optimization; (c) time optimization; (d) solvent screening; (e) TBHP amount optimization; reaction conditions: 4-nitrobenzaldehyde (**1e**, 0.5 mM, 76 mg), morpholine (**2a**, 0.5 mM, 43 μL), 5–6 M TBHP in dodecane (112 μL, ~0.5 mM), **ZN-O-A-7** (7.1 mol%, 10 mg) catalyst, tetrahydrofuran (3 mL), and stirred at 90 °C up to 2 h.

Optimization of the reaction conditions

To begin our studies, we selected 4-nitrobenzaldehyde (**1e**, 0.5 mM, 76 mg) and morpholine (**2a**, 0.5 mM, 43 μL) as substrates, 5–6 M TBHP in dodecane (112 μL, ~0.5 mM) as the oxidant, **ZN-O-A-7** as the catalyst, and tetrahydrofuran (THF) as the solvent (Fig. 3). Various parameters including catalyst loading, reaction time, oxidant concentration, solvent, and oxidant were thoroughly screened to optimize the reaction conditions. 4-Nitrobenzaldehyde (**1e**) and morpholine (**2a**) were quantitatively converted to morpholino(4-nitrophenyl) methanone (**3e**) and *tert*-butyl 4-nitrobenzoate (**8e**) using a **ZN-O-A-7** catalyst (7.1 mol%) in the presence of TBHP (0.5 mM) in 3 mL of tetrahydrofuran (THF), and stirred at 90 °C for two hours. A variety of materials derived from both **ZN-O** and **ZN-R** parent structures were evaluated for their performance. Notably, all materials, except for **ZN-O**, which contained approximately a 50/50 ratio of Ni(II)/Ni(0), exhibited moderate yields with low selectivity suggesting the cooperativity between the active sites of the heterostructure ZnO–NiO–Ni (**ZN-O-A-7**) material is important for the oxidative amidation reaction (Fig. 3a). The conversion and selectivity of the corresponding product gradually decreased as catalyst mol% was reduced. Moreover, the optimal amount of the catalyst (**ZN-O-A-7**) was determined (Fig. 3b). The progression of the reaction over time was monitored. A 24% initial conversion took place within 10 minutes, and the conversion continued to increase gradually over time. Complete conversion of the reactant into the product was achieved within 2 hours (Fig. 3c). Solvents had a significant impact on reaction yield as well as product selectivity. The solvent optimization suggests that the yield of the corresponding amide is higher in THF as compared with moderate and lower yield in dioxane and DMF respectively. Furthermore, the lower yield was obtained in a protic solvent such as methanol (Fig. 3d).

Optimization of the oxidant shows that *tert*-butyl hydroperoxide (TBHP) provided excellent conversion with high selectivity towards the corresponding amide product, whereas hydrogen peroxide (H_2O_2) yielded a lower product yield. Furthermore, the amount of TBHP required for the reaction was optimized which suggests the lower amount (0.26 mM, 0.34 mM, and 0.43 mM) gave moderate yield with reduced selectivity, while a 0.5 mM quantity was found optimal for achieving complete conversion with high selectivity (Fig. 3e).

Substrate scope

The versatility of this method was widely studied for various benzaldehyde derivatives within the optimized reaction

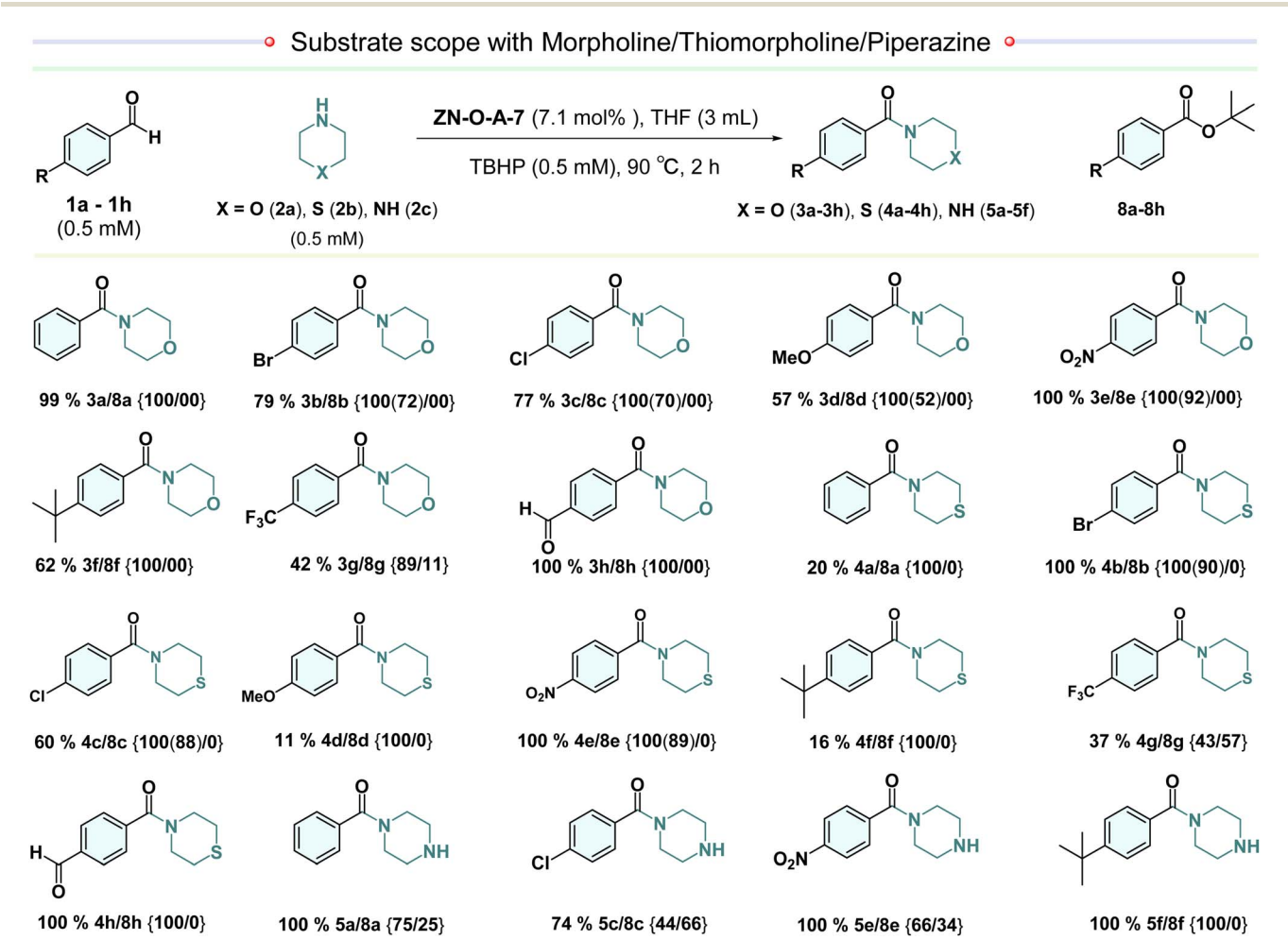

Fig. 4 Substrate scope with morpholine/thiomorpholine/piperazine. The yields indicated within parentheses represent the isolated yield.

conditions. Thus, the benzaldehyde derivatives underwent the oxidative amidation reaction with morpholine in the presence of the **ZN-O-A-7** (10 mg, 7.1 mol%) catalyst and TBHP (0.5 mM) as the oxidant at 90 °C in a closed vessel for 1.5–3 h (Fig. 4). Overall, the method demonstrated excellent conversions, showing high selectivity in favor of the formation of the corresponding amides **3a** to **3h**. Remarkably, both electron-rich and electron-deficient benzaldehyde derivatives consistently yielded the corresponding amides **3a** to **3h** (Fig. 4). Various functional groups, including Br (**3b**), Cl (**3c**), and F (**3g**), remained unaffected during the catalytic process, leading to the generation of their respective amides with high conversion and selectivity under the optimized reaction conditions. Significantly, even sensitive groups such as nitro (NO_2) were well tolerated as substituents, resulting in the exclusive formation of the corresponding product **3e** (Fig. 4). Continuing our investigation, the scope of our study was expanded to include other secondary amines such as thiomorpholine and piperazine. This expansion aims to systematically explore and explain the wider applicability and potential of the developed method. Gratifyingly, various benzaldehydes underwent complete conversion, yielding the respective amides **4a** to **4h** and **5a**, **5c**, **5e**, and **5f** (refer to Fig. 4), demonstrating good conversions and selectivity. Different functional groups, such as Br (**4b**), Cl (**4c** and **5c**), and F (**4g**), were tolerated under the catalytic process, resulting in the formation of their corresponding amides with good conversion and selectivity (Fig. 4). Furthermore, the reaction conditions exhibited tolerance towards sensitive functional groups like nitro (NO_2), allowing for the formation of the corresponding products **4e** and **5e** with good conversion (Fig. 4 and S1–S12†).

The protocol demonstrates robustness across various benzaldehydes and secondary amines (morpholine, thiomorpholine, and piperazine). Consequently, we expanded our investigation to include pyrrolidine and piperidine, promoting the study of their applicability. As previously observed, the catalyst heterostructure ZnO–NiO–Ni (**ZN-O-A-7**) converts a reactant into its corresponding amides **6a** to **6g** and **7a** to **7f** with moderate to good conversion (Fig. 5). Diverse functional groups, including Br (**6b** and **7b**), Cl (**6c** and **7c**), and F (**6g**), showed versatility under the catalytic process, leading to the formation of their respective amides with notable conversion and selectivity. Moreover, we successfully conducted the oxidative amidation of both heterocyclic and aliphatic aldehydes using morpholine and thiomorpholine, resulting in the production of corresponding amides (**9a** to **13a**) with good conversion and selectivity (Fig. 5 and S13–S23†).

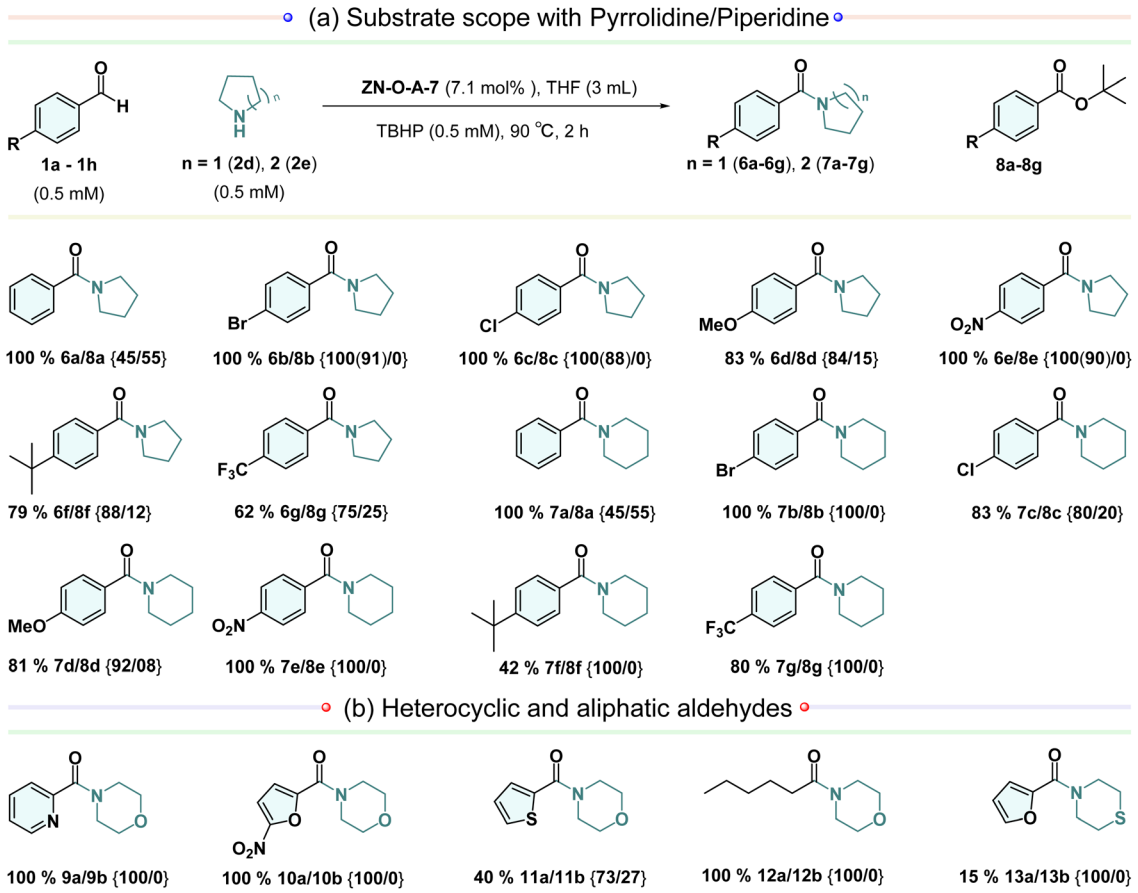

Fig. 5 Substrate scope (a) with pyrrolidine/piperidine; (b) with heterocyclic and aliphatic aldehydes. The yields indicated within parentheses represent the isolated yield.

Role of cooperativity and mechanism

A model reaction was performed with TEMPO (2,2,6,6-tetramethyl-1-piperidinyloxy) and BHT (butylated hydroxytoluene) acting as a free radical scavenger to determine whether the reaction progresses through the ionic or free radical pathway (Fig. 6a(1)). Notably, in both the reagents, the

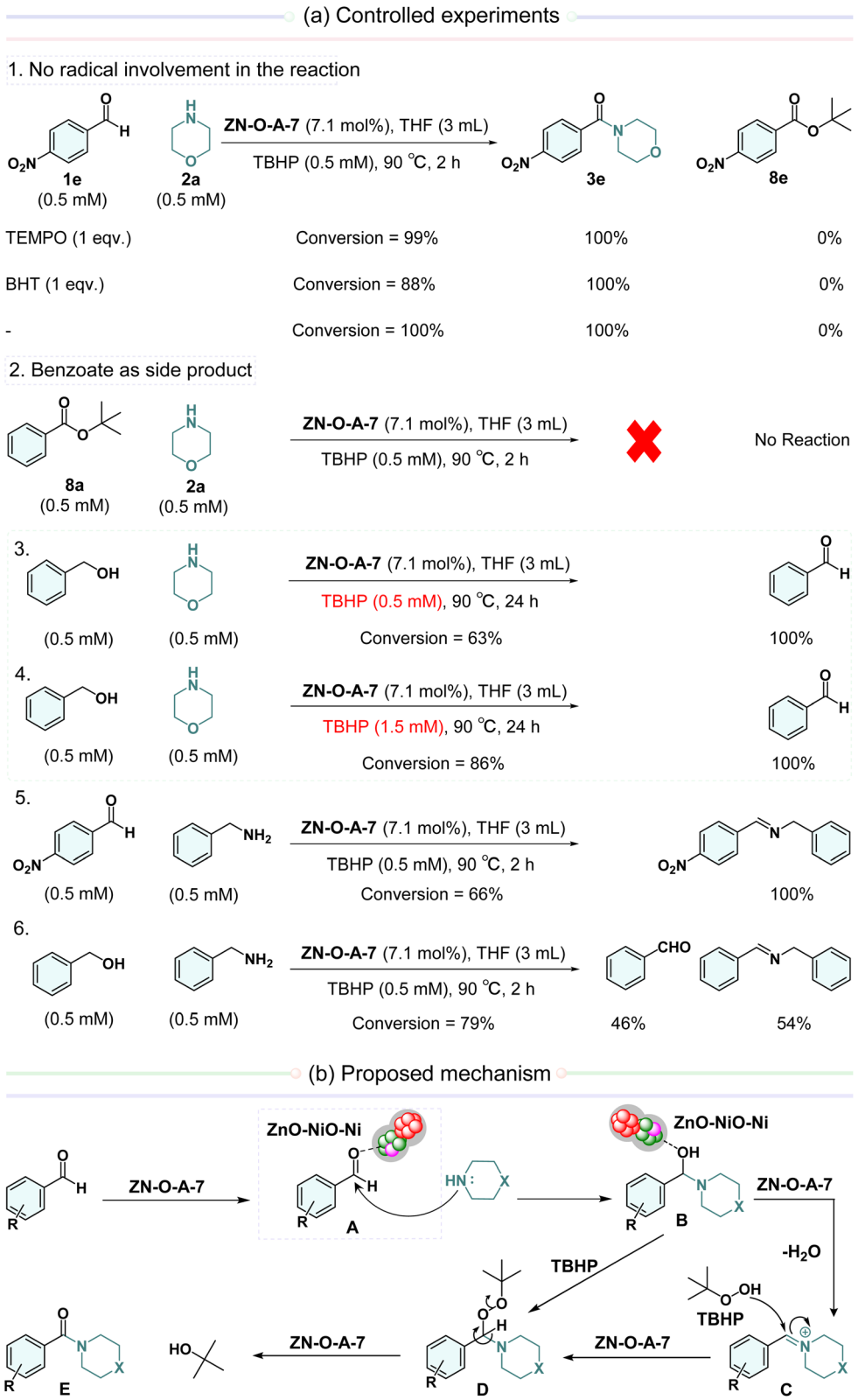

Fig. 6 Mechanistic investigation: (a) controlled experiments; (b) proposed mechanism.

corresponding amide **3e** was formed with 100% selectivity, while conversions of 99% and 88% were observed, suggesting that the reaction proceeded *via* the ionic pathway. In the substrate scope described above (Fig. 4 and 5), benzoate products were observed with certain substrates. Therefore, *tert*-butyl benzoate (**8a**) was synthesized following the reported procedure[37] (Fig. S24 and S25†) and subjected to a reaction using our optimized conditions. Remarkably, no product was formed using the benzoate substrate, indicating that benzoate serves as a side product rather than an intermediate in the reaction (Fig. 6a(2)). Furthermore, instead of benzaldehyde, we did the reaction using benzyl alcohol with morpholine under optimized conditions to obtain only benzaldehyde as a product rather than its corresponding amide (Fig. 6a(3)). Additionally, we increased the amount of TBHP (3 eq.), leading to a slight increase in benzaldehyde conversion; however, no formation of amide product was observed (Fig. 6a(4)). Additionally, we examined the reaction of 4-nitrobenzaldehyde (**1e**) with benzylamine under our optimized conditions, resulting in the selective formation of the corresponding imine with a 66% conversion (Fig. 6a(5)). Moreover, we performed a reaction between benzyl alcohol and benzylamine under optimized reaction conditions, resulting in the formation of 46% benzaldehyde and 54% imine with overall conversion of 79% (Fig. 6a(6)).

The controlled studies suggested that the corresponding amide was obtained through an ionic mechanism rather than a radical mechanism (Fig. 6a(1)). The active **ZN-O-A-7** catalyst contains distinct heterojunctions between ZnO, NiO, and Ni in which robust charge transfer enhances the binding of benzaldehyde to one of the Lewis acidic active sites of the catalyst, thereby increasing the electrophilicity of the carbonyl group of benzaldehyde (depicted as **A** in Fig. 6b).[38] This facilitates the easy attack of the secondary amine on the carbonyl group, leading to the formation of a hemiaminal intermediate (**B**) as shown in the proposed mechanism (Fig. 6b). Based on the literature reports[39–42] and our observation, the hemiaminal intermediate (**B**) can produce an amide (**E**) either through an imine (**C**) intermediate or direct attack of TBHP on intermediate **B**. The Lewis acidic active sites of the **ZN-O-A-7** catalyst can facilitate the formation of an iminium ion (**C**) from the hemiaminal intermediate **B** without generating radicals, which can undergo nucleophilic attack from TBHP leading to the formation of an amide (**E**) and *tert*-butanol through intermediate **D**. The **ZN-O-A-7** catalyst plays a crucial role in oxidative amidation,

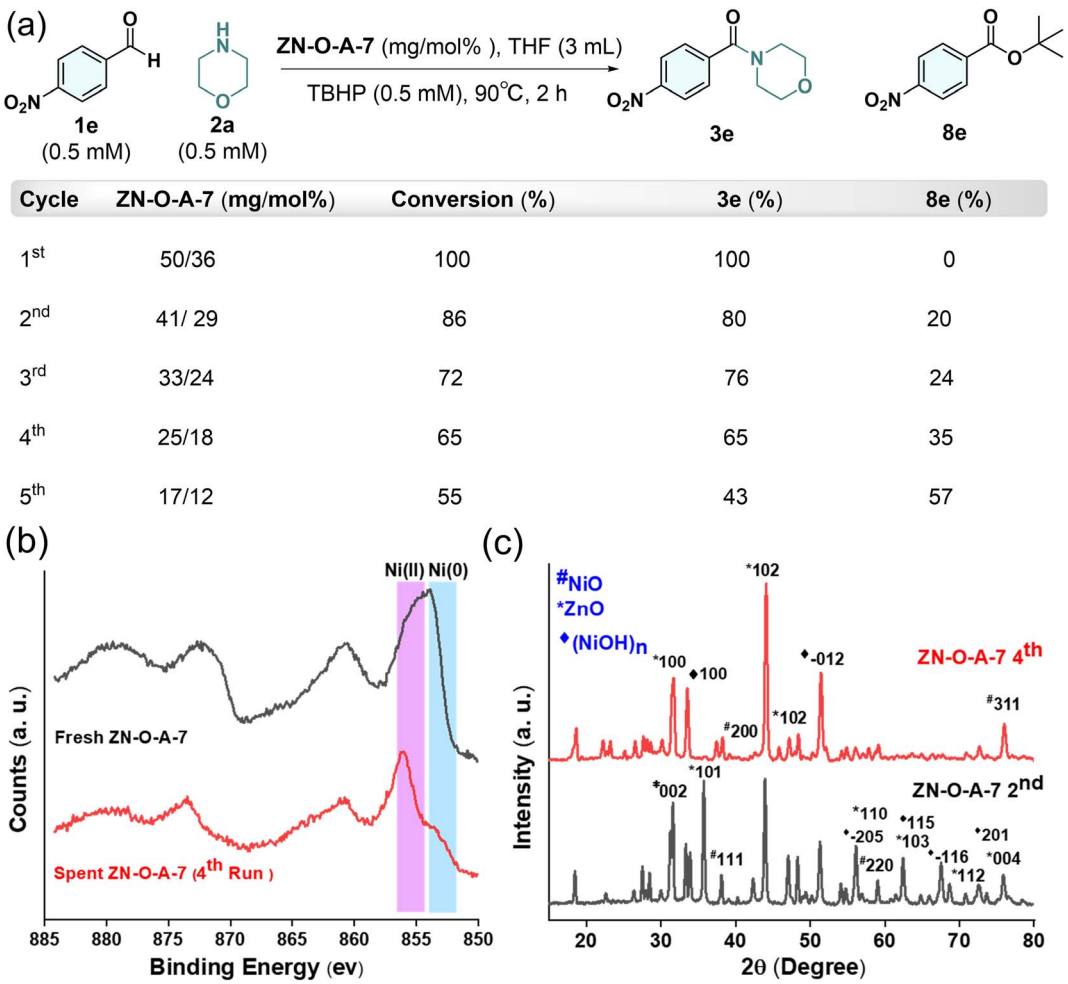

Cycle	ZN-O-A-7 (mg/mol%)	Conversion (%)	3e (%)	8e (%)
1st	50/36	100	100	0
2nd	41/ 29	86	80	20
3rd	33/24	72	76	24
4th	25/18	65	65	35
5th	17/12	55	43	57

Fig. 7 (a) Reusability study of ZN-O-A-7 promoted oxidative amidation; (b) comparative high-resolution XPS Ni 2p between fresh and spent ZN-O-A-7; (c) PXRD data of spent ZN-O-A-7 after the 2nd and 4th runs.

mainly through its Lewis acidic sites. These sites coordinate with the OH group of the hemiaminal intermediate (**B**), facilitating its transformation into a more reactive leaving group. Subsequently, either TBHP can directly attack to form intermediate **D**, or the amine nitrogen's lone pair can intramolecularly attack, leading to the conversion of the hemiaminal intermediate into the corresponding imine (**C**).

Practicability of the catalyst

We investigated the yield and leaching properties of the **ZN-O-A-7** promoted oxidative amidation reaction to measure its performance under optimum reaction conditions and evaluate its efficiency, stability, selectivity, and reusability. The catalyst was recovered by centrifugation following each reaction for the reusability studies. It subsequently underwent two methanol washes and was vacuum-dried to get ready for the following set of reactions using fresh substrates and reagents. Regarding both yield and selectivity, the efficiency of the spent catalysts (**ZN-O-A-7**) exhibited no significant decline up to the 3rd run.

However, a notable reduction in both yield and selectivity was observed during the 4th and 5th runs (Fig. 7a). There was more leaching of zinc than nickel under oxidizing conditions, based on the ICP-MS analysis of **ZN-O-A-7** after the second and fourth runs. The spent **ZN-O-A-7** after the fourth run revealed that, in the presence of oxidizing reaction conditions, Ni(0) was converted to Ni(II) (Fig. 7b). The PXRD analysis of spent **ZN-O-A-7** provided more evidence that nickel hydroxide [$Ni(OH)_n$] was produced. After the third run, the reaction yield and selectivity decreased because [$Ni(OH)_n$] inhibited the oxidation reaction (Fig. 7c and S26 and S27†).

It is crucial to evaluate the benefits and limitations of catalytic chemical transformations, focusing on their environmental and sustainability aspects. This evaluation should be guided by the fundamental principles of green chemistry, known as "the 12 principles of green chemistry".[43] To evaluate the sustainability and environmental advantages of our one-step oxidative amidation reaction, we compared our methodology with previously reported catalytic oxidative amidation reactions using the CHEM21 green metrics toolkit. Developed by Clark *et al.*,[44] this quantitative tool extends "the 12 principles of green chemistry". Several chemical transformations have been analyzed using this toolkit.[45–47] Compared to the selected reported methods using Pd nanoparticles,[27] Cu-MOF,[28] CoO nanoparticles,[29] and NiO@Ni[30] catalysts, which require excess oxidants and display moderate RME, our method excels in yield, atom economy (AE), and reaction mass efficiency (RME) using a stoichiometric amount of oxidant in a moderately good solvent (THF). This highlights the higher efficiency and sustainability of our approach (Fig. S28–S37†).

Conclusion

In summary, we have developed a highly efficient and sustainable method for synthesizing amides *via* oxidative amidation reactions using well-defined nanoscale heterojunctions [ZnO–NiO–Ni] (**ZN-O-A-7**) as the catalyst and *tert*-butyl hydroperoxide (TBHP) as the oxidant. Our study highlights the crucial role of the ZnO–NiO–Ni heterostructure in enhancing both the efficiency and selectivity of the oxidative amidation between aldehydes and secondary amines. We have extensively explored the versatility of our protocol across various aldehyde derivatives and secondary amines, including morpholine, thiomorpholine, piperazine, pyrrolidine, and piperidine. Additionally, mechanistic studies involving controlled experiments have shown that charge relocalization within the ZnO–NiO–Ni heterojunction generates Lewis acidic active sites, which plays a crucial role in catalyzing the reaction between aldehydes and secondary amines, leading to the formation of a hemiaminal intermediate. This intermediate is subsequently oxidized into the corresponding products in the presence of TBHP and the catalyst. The catalysts exhibited high activity, excellent reusability, a wide substrate scope, and notable functional group tolerance for oxidative amidation reactions. We evaluated the sustainability of our methodology using the CHEM21 green metrics toolkit, which demonstrated that our yield, atom economy (AE), and reaction mass efficiency (RME) were excellent compared to other reported methodologies.

Data availability

The data supporting this article have been included as part of the ESI.†

Author contributions

A. R. S. – writing – original draft, investigation, formal analysis, visualization. R. D. P. – writing – original draft, investigation, methodology, formal analysis, visualization. S. P. – supervision, funding acquisition, writing – review & editing.

Conflicts of interest

The authors declare no competing financial interest.

Acknowledgements

Financial support of this work by DST-SERB (project no. CRG/2021/002384), CSIR (A. R. S. for SRF) and DST-Inspire (R. D. P. for SRF) is gratefully acknowledged. The Analytical and Environmental Science Division and Centralized Instrument Facility of CSIR-CSMCRI are acknowledged for providing instrument facilities. The CSIR-CSMCRI communication number is 127/2024.

References

1 A. K. Ghose, V. N. Viswanadhan and J. J. Wendoloski, *J. Comb. Chem.*, 1999, **1**, 55–68.
2 V. R. Pattabiraman and J. W. Bode, *Nat.*, 2011, **480**, 471–479.
3 S. Kumari, A. V. Carmona, A. K. Tiwari and P. C. Trippier, *J. Med. Chem.*, 2020, **63**, 12290–12358.
4 J. S. Carey, D. Laffan, C. Thomson and M. T. Williams, *Org. Biomol. Chem.*, 2006, **4**, 2337–2347.

5 L. Crespo, G. Sanclimens, M. Pons, E. Giralt, M. Royo and F. Albericio, *Chem. Rev.*, 2005, **105**, 1663–1682.
6 G. Evano, N. Blanchard and M. Toumi, *Chem. Rev.*, 2008, **108**, 3054–3131.
7 R. M. de Figueiredo, J.-S. Suppo and J.-M. Campagne, *Chem. Rev.*, 2016, **116**, 12029–12122.
8 A. Leggio, E. L. Belsito, G. De Luca, M. L. Di Gioia, V. Leotta, E. Romio, C. Siciliano and A. Liguori, *RSC Adv.*, 2016, **6**, 34468–34475.
9 L. J. Gooßen, D. M. Ohlmann and P. P. Lange, *Synth.*, 2009, **2009**, 160–164.
10 Y. Shimizu, H. Morimoto, M. Zhang and T. Ohshima, *Angew. Chem.*, 2012, **51**, 8564–8567.
11 T. K. Houlding, K. Tchabanenko, M. T. Rahman and E. V. Rebrov, *Org. Biomol. Chem.*, 2013, **11**, 4171–4177.
12 J. R. Dunetz, J. Magano and G. A. Weisenburger, *Org. Process Res. Dev.*, 2016, **20**, 140–177.
13 C. L. Allen, A. R. Chhatwal and J. M. J. Williams, *Chem. Commun.*, 2012, **48**, 666–668.
14 A. Alanthadka and C. U. Maheswari, *Adv. Synth. Catal.*, 2015, **357**, 1199–1203.
15 N. Jiao and S. S. Stahl, *Green Oxidation in Organic Synthesis*, 2019.
16 A. S. Santos, A. M. S. Silva and M. M. B. Marques, *Eur. J. Org Chem.*, 2020, **2020**, 2501–2516.
17 M. T. Sabatini, L. T. Boulton, H. F. Sneddon and T. D. Sheppard, *Nat. Catal.*, 2019, **2**, 10–17.
18 K. Nakagawa, S. Mineo, S. Kawamura, M. Horikawa, T. Tokumoto and O. Mori, *Synth. Commun.*, 1979, **9**, 529–534.
19 A. Álvarez-Pérez, M. A. Esteruelas, S. Izquierdo, J. A. Varela and C. Saá, *Org. Lett.*, 2019, **21**, 5346–5350.
20 S. Roy, S. Roy and G. W. Gribble, *Tetrahedron*, 2012, **68**, 9867–9923.
21 M. Albert-Soriano and I. M. Pastor, *Eur. J. Org Chem.*, 2016, **2016**, 5180–5188.
22 T. Truong, G. H. Dang, N. V. Tran, N. T. Truong, D. T. Le and N. T. S. Phan, *J. Mol. Catal. A*, 2015, **409**, 110–116.
23 A. M. Whittaker and V. M. Dong, *Angew. Chem., Int. Ed.*, 2015, **54**, 1312–1315.
24 J.-F. Soulé, H. Miyamura and S. Kobayashi, *Chem.–Asian J.*, 2013, **8**, 2614–2626.
25 W. Ali, S. K. Rout, S. Guin, A. Modi, A. Banerjee and B. K. Patel, *Adv. Synth. Catal.*, 2015, **357**, 515–522.
26 Y.-X. Xie, R.-J. Song, X.-H. Yang, J.-N. Xiang and J.-H. Li, *Eur. J. Org Chem.*, 2013, **2013**, 5737–5742.
27 S. Rostamnia, E. Doustkhah, H. Golchin-Hosseini, B. Zeynizadeh, H. Xin and R. Luque, *Catal. Sci. Technol.*, 2016, **6**, 4124–4133.
28 S. Jamalifard, J. Mokhtari and Z. Mirjafary, *RSC Adv.*, 2019, **9**, 22749–22754.
29 F. Rajabi, M. Raessi, R. A. D. Arancon, M. R. Saidi and R. Luque, *Catal. Commun.*, 2015, **59**, 122–126.
30 B. Goel, V. Vyas, N. Tripathi, A. Kumar Singh, P. W. Menezes, A. Indra and S. K. Jain, *ChemCatChem*, 2020, **12**, 5743–5749.
31 P. Ghamari kargar, G. Bagherzade and H. Beyzaei, *Mol. Catal.*, 2022, **526**, 112372.
32 D. Huang, H. Sun, J. Li, H. Xu and H. Zhao, *ChemCatChem*, 2023, **15**, e202300715.
33 O. T. K. Nguyen, V. H. Nguyen and L. X. Nong, *J. Chem. Biotechnol.*, 2023, **98**, 2707–2715.
34 D. Astruc, *Chem. Rev.*, 2020, **120**, 461–463.
35 A. R. Shelte, R. D. Patil, S. Karan, G. R. Bhadu and S. Pratihar, *ACS Appl. Mater. Interfaces*, 2023, **15**, 24329–24345.
36 A. R. Shelte, R. N. Khatal and S. Pratihar, *Appl. Catal.*, 2023, **666**, 119417.
37 D. T. Racys, J. Eastoe, P.-O. Norrby, I. Grillo, S. E. Rogers and G. C. Lloyd-Jones, *Chem. Sci.*, 2015, **6**, 5793–5801.
38 S. Pratihar, *Org. Biomol. Chem.*, 2016, **14**, 2854–2865.
39 H. Miyamura, H. Min, J.-F. Soulé and S. Kobayashi, *Angew. Chem., Int. Ed.*, 2015, **54**, 7564–7567.
40 C. Chen and S. H. Hong, *Org. Biomol. Chem.*, 2011, **9**, 20–26.
41 Y. F. Guo, T. L. Ren, B. H. Xu, Y. F. Wang and S. J. Zhang, *Asian J. Org. Chem.*, 2016, **5**, 568–574.
42 A. K. Padala, N. Mupparapu, D. Singh, R. A. Vishwakarma and Q. N. Ahmed, *Eur. J. Org Chem.*, 2015, **2015**, 3577–3586.
43 A. Ivanković, A. Dronjić, A. M. Bevanda and S. Talić, *Int. J. Sustainable Energy*, 2017, **6**, 39–48.
44 C. R. McElroy, A. Constantinou, L. C. Jones, L. Summerton and J. H. Clark, *Green Chem.*, 2015, **17**, 3111–3121.
45 R. D. Patil and S. Pratihar, *ACS Sustainable Chem. Eng.*, 2024, **12**, 6206–6219.
46 M. Prieschl, J. García-Lacuna, R. Munday, K. Leslie, A. O'Kearney-McMullan, C. A. Hone and C. O. Kappe, *Green Chem.*, 2020, **22**, 5762–5770.
47 M. A. Droesbeke and F. E. Du Prez, *ACS Sustain. Chem. Eng.*, 2019, **7**, 11633–11639.